

Preparation and Characterisation of Silica-Coated Iron Oxide Nanoparticles ($\text{Fe}_3\text{O}_4@\text{SiO}_2\text{-NPs}$)

Nurul Izza Taib^{1*}, Famiza Abdul Latif² and Nur Diyana Syazwani Zambri²

¹Faculty of Applied Sciences, Universiti Teknologi MARA, Perak Branch, Tapah Campus, Tapah Road, 35400 Perak, Malaysia

²Faculty of Applied Sciences, Universiti Teknologi MARA, 40450 Shah Alam, Selangor, Malaysia

*Corresponding author's e-mail: izza257@uitm.edu.my

Received: 26 November 2020

Accepted: 10 February 2021

Online first: 1 April 2021

ABSTRACT

Iron oxide nanoparticles ($\text{Fe}_3\text{O}_4\text{-NP}_s$) were synthesized in ammonium hydroxide medium using neem leaf extract as a reducing agent through a co-precipitation method. SiO_2 has been coated on the surface of Fe_3O_4 ($\text{Fe}_3\text{O}_4@\text{SiO}_2$) by hydrolysis and condensation of tetraethyl orthosilicate (TEOS) under alkaline medium conditions at 80°C . The properties of the resulting nanoparticles were analysed by transmission electron microscopy (TEM), fourier transform infrared (FTIR) field emission scanning electron microscopy (FESEM), energy-dispersive X-rays spectroscopy (EDX) and vibrating sample magnetometry (VSM). It was found that only 500 L TEOS was required to obtain the best coating on Fe_3O_4 core structures. TEM micrographs show the formation of multiple cores of iron oxide nanoparticles within the silica matrix. FTIR analyses show the formation of Si-O-Si bonds at $1084.2\text{--}1101.4\text{ cm}^{-1}$ hence confirming that Fe_3O_4 core was successfully coated by SiO_2 . From FESEM analysis, the average size of silica was found to be $\sim 50\text{--}70\text{ nm}$. EDX of the $\text{Fe}_3\text{O}_4@\text{SiO}_2$ confirmed that silica had been successfully coated on the surface of Fe_3O_4 . VSM measurements revealed the superparamagnetic properties of $\text{Fe}_3\text{O}_4@\text{SiO}_2$ that is desirable for biomedical applications.

Keywords: iron oxide nanoparticles, magnetite, silica, VSM (vibrating sample magnetometer), superparamagnetic



INTRODUCTION

Iron oxide nanoparticles (IONPs) have been a topic of intense research owing to their biocompatibility, high surface area to volume ratio, nanosized, superparamagnetic, physical and chemical stability. Also, IONPs collectively is the only nanomaterial to have received approval from the Food and Drug Association (FDA) indicating it is safe for clinical use [1]. IONPs have the ability to induce magnetisation by applying an external magnetic field and do not exhibit any magnetism once the external magnetic field is removed. This unique characteristic allows them to be guided towards a target site and be heated by applying external alternating magnetic field [1, 2]. Pertaining to these properties, the appeals for IONPs are growing for different applications including targeted drug delivery, disease therapy by magnetic hyperthermia or contrast agents for magnetic resonance imaging (MRI) [1-4]. They have the ability to degrade through various metabolic pathways in the body. Thus, leaching of the iron does not cause any major side effects [5, 6].

However, uncoated IONPs are not stable in normal physiological conditions [7]. They tend to aggregate in order to reduce their surface energy. As a result, the aggregation processes significantly decrease the IONPs interfacial area, thus resulting in the loss of dispersibility. Thus, IONPs need to be stabilised with polymer-based surfactants (such as dextran, polysaccharides, PEG) as well as mesoporous silica surface functionalisation [2, 8]. The stabilisation procedure provides IONPs a good dispersion, increases the protection and shields the particles from environment conditions such as oxidation [1, 2].

Silica are widely used for coating oxide nanoparticles as they were able to form stable, biocompatible shells to help minimise agglomeration [1, 2, 8] by screening the magnetic dipolar attraction among the nanoparticles. In fact, surface silica could be made rich in silanol groups and help further to stabilise the nanoparticle via surface modification through reactions between the silanol groups and biological entities and this could lead to numerous applications in the biomedical fields.

According to the US Food and Drug Administration (FDA), silica is 'generally considered as safe' for consumption [9]. Silica coated IONPs

are mechanically stable with definite structures that are able to store and release the biomolecules/drug on the specific target. They are also very resistant to hydrolysis degradation as well as pH, heat, and mechanical stress [10]. The synergy uses of silica and iron oxide nanoparticles as magnetic silica nanoparticles received enormous attention due to their potential for simultaneous magnetic resonance imaging (MRI) detection and drug targeting delivery [11-14]. It is essential to synthesize silica coated Fe_3O_4 -NPs having various particle sizes using the similar synthetic route. The variation in condensation of silica, or oxidation of Fe_3O_4 NPs are the crucial aspects to control the magnetisation property of Fe_3O_4 -NPs as it is very important for different biological applications [15].

Herein, superparamagnetic iron oxide (Fe_3O_4) nanoparticles were synthesized using neem leaf extract according to a published procedure [16]. In our previous papers [16,17], the preparation and characterisation of superparamagnetic Fe_3O_4 -NPs (9–14 nm) have been achieved through a co-precipitation process based on a green and facile approach.

In this work, Fe_3O_4 nanoparticles were used as a core material for the fabrication of silica-coated iron oxide nanoparticles ($\text{Fe}_3\text{O}_4@\text{SiO}_2$). The method involves growing silica directly onto the iron oxide via the hydrolysis and condensation of tetraethyl orthosilicate (TEOS) under alkaline medium at 80°C . Then, the cetyltrimethylammonium bromide (CTAB) was removed by solvent extraction, in the presence of alcoholic solutions of ammonium nitrate (20 mg/L) at 60°C for 30 minutes. Results from the morphological, FTIR and magnetic analyses were studied and compared. In this study, the volume of TEOS used in the silica coating was varied in the range of $100\mu\text{L}$ to $900\mu\text{L}$, while the other parameters were held constant.

EXPERIMENTAL

Preparation of Neem Leaves Extract

Neem leaves extract was prepared according to a method reported by Taib *et al.* [16]. 5 g of neem leaf powder were mixed with distilled water

and the mixture was heated at 80°C. Then, the mixture was filtered, and the obtained extract was stored at 4°C for further use.

Synthesis of Iron Oxide Nanoparticles (Fe₃O₄-NPs)

Iron oxide nanoparticles were prepared via a co-precipitation method according to a published procedure [16] by using neem leaves extract as a green reducing agent. FeCl₂.4H₂O and FeCl₃.6H₂O were mixed with a ratio of 1:2 under nitrogen atmosphere. The mixture was heated at 80°C followed by the addition of 5 mL of neem leaf extract and 20 mL of 25% of ammonium hydroxide. The black precipitate obtained were finally centrifuged and washed with distilled water for further use.

Synthesis of Fe₃O₄@SiO₂-NPs

An aqueous solution of iron oxide nanoparticles was prepared by mixing 500 μL of synthesized iron oxide nanoparticles (Fe₃O₄) with 5 mL distilled water (H₂O) of 100 mg cetyltrimethylammonium bromide (CTAB) in beaker. The solution was stirred vigorously for 30 minutes resulting in a black Fe₃O₄-CTAB suspension. In order to create a SiO₂ coating layer around the Fe₃O₄-CTAB, the solution was then added into a propylene bottle containing 40 mL H₂O and 350 μL of 2M sodium hydroxide (NaOH) heated at 80°C. Then, 100 μL tetraethylorthosilicate (TEOS) and 3.00 mL of ethyl acetate was added to the reaction solution in sequence under rapid stirring. The solution was further stirred for two hours while maintaining the temperature at 80°C to give rise to a light brown precipitate. After cooling, a light brown solid product was isolated by centrifugation and washed thrice with ethanol in order to remove unreacted species. To control the thickness of silica shell, the amount of TEOS was varied (300 μL, 500 μL, 700 μL and 900 μL). The surfactant template (CTAB) was removed from the mesopore channels by refluxing the Fe₃O₄@SiO₂ in alcoholic solutions of NH₄NO₃ (20 mg/mL) at 60°C for 30 minutes. The obtained light-brown solid was allowed to cool down, centrifuged, and washed thrice with ethanol and finally dried in air. The obtained samples were denoted as C1, C3, C5, C7 and C9, which indicates different amounts of TEOS, respectively (see Table 1).

Table 1: Parameters for Synthesis of Fe₃O₄@SiO₂-NPs

Samples	V _{TEOS} (μL)	V _{IONPs} (μL)	V _{NaOH} (μL)	V _{ethyl acetate} (μL)
C1	100	500	350	3000
C3	300	500	350	3000
C5	500	500	350	3000
C7	700	500	350	3000
C9	900	500	350	3000

Characterisation of Fe₃O₄@SiO₂-NPs

The size and morphology of Fe₃O₄@SiO₂-NPs were identified by transmission electron microscopy (TEM) using a Technai G2 20S Twin TEM operating at 200kV (Eindhoven, Netherland). Fourier transform infrared (FTIR) spectra were recorded using the KBr pellet method over the range of 4000–400 cm⁻¹ with a Spectrum One FTIR spectrophotometer (Perkin Elmer). The magnetic properties of NPs were evaluated by a vibrating sample magnetometer (Lake Shore 7404) under external magnetic fields up to ±14000 Oe at 300 K. Field emission scanning electron microscope (FESEM) were carried out on a JEOL 2010 Field Emission Scanning Electron Microscope (FESEM) coupled with an energy dispersive X-ray spectrometer (EDX) (ZEISS supra 40VP).

RESULTS AND DISCUSSION

Fourier Transform Infrared (FTIR) Spectroscopy

The FTIR spectra of the iron oxide nanoparticles (Fe₃O₄-NPs), Fe₃O₄@SiO₂ with different volumes of TEOS and Fe₃O₄@SiO₂ after CTAB removal are illustrated in Figure 1. There are two main absorptions centered around 505 and 3416 cm⁻¹ observed in Figure 1(a), were attributed to Fe–O–Fe and O–H stretching vibration respectively. The strong absorption band around 3416 cm⁻¹ may also come from the NH stretching vibration of amines in the neem leaf extract. The adsorption peak at 1633 cm⁻¹ may be assigned to amide C=O stretching, indicating the presence of –COOH group in the neem leaf extract. The peak at 2429 cm⁻¹ was the symmetric stretching vibration

of CH₂ due to alkyne groups present in the phytoconstituents of extracts. These observations indicated the presence of flavanones or terpenoids molecules of neem leaf extract in the Fe₃O₄-NPs. The result agrees with that of previous work [18].

Compared to the bare Fe₃O₄-NPs, additional absorption peaks at 1084 and 1101 cm⁻¹ were linked to the asymmetric vibrations of siloxane groups (Si–O–Si) with Si–O bending at 789.7 cm⁻¹ and O–H from water adsorbed on the silanol surface of silica at 1643.1 cm⁻¹ (see Figure 1 (b)-(g)), signifying that silica has been successfully grafted onto the surface of Fe₃O₄-NPs. The broad band around 3844-3400 cm⁻¹ can be assigned to O–H bonds of surface silanols and adsorbed water molecules. The bands at 965.9 cm⁻¹ reveal the stretching of vibrations of the silanols groups (Si–OH) on the silica surface, which arises from the TEOS compound. The intensity of this peak increases as the amount of TEOS increases. The observation found in the FTIR spectra for the samples prepared are in good agreement with those found in literature reports [19-21].

The encapsulation of Fe₃O₄ core by silica was evidenced by the presence of both Si–O vibrations and Fe–O after the silica coating. The bands at 471.5-553.2 cm⁻¹ shifted to the higher wavenumber increasing TEOS content, indicating the presence of an asymmetric stretching vibration due to Fe–O–Si (Figure 1) [22]. The FTIR spectra of the Fe₃O₄@SiO₂-NPs consisting the peak of CTAB at 2922.4 cm⁻¹ and 2857.8 cm⁻¹ corresponding to -CH₂- stretching bands of the alkyl group. The absence of this peak (see Figure 1 (g)) in the samples suggests the successful removal of CTAB via solvent extraction [19]. The data suggests that there are no significant structure differences among C1, C3, C5, C7, C9 particles and Fe₃O₄@SiO₂ after CTAB removal.

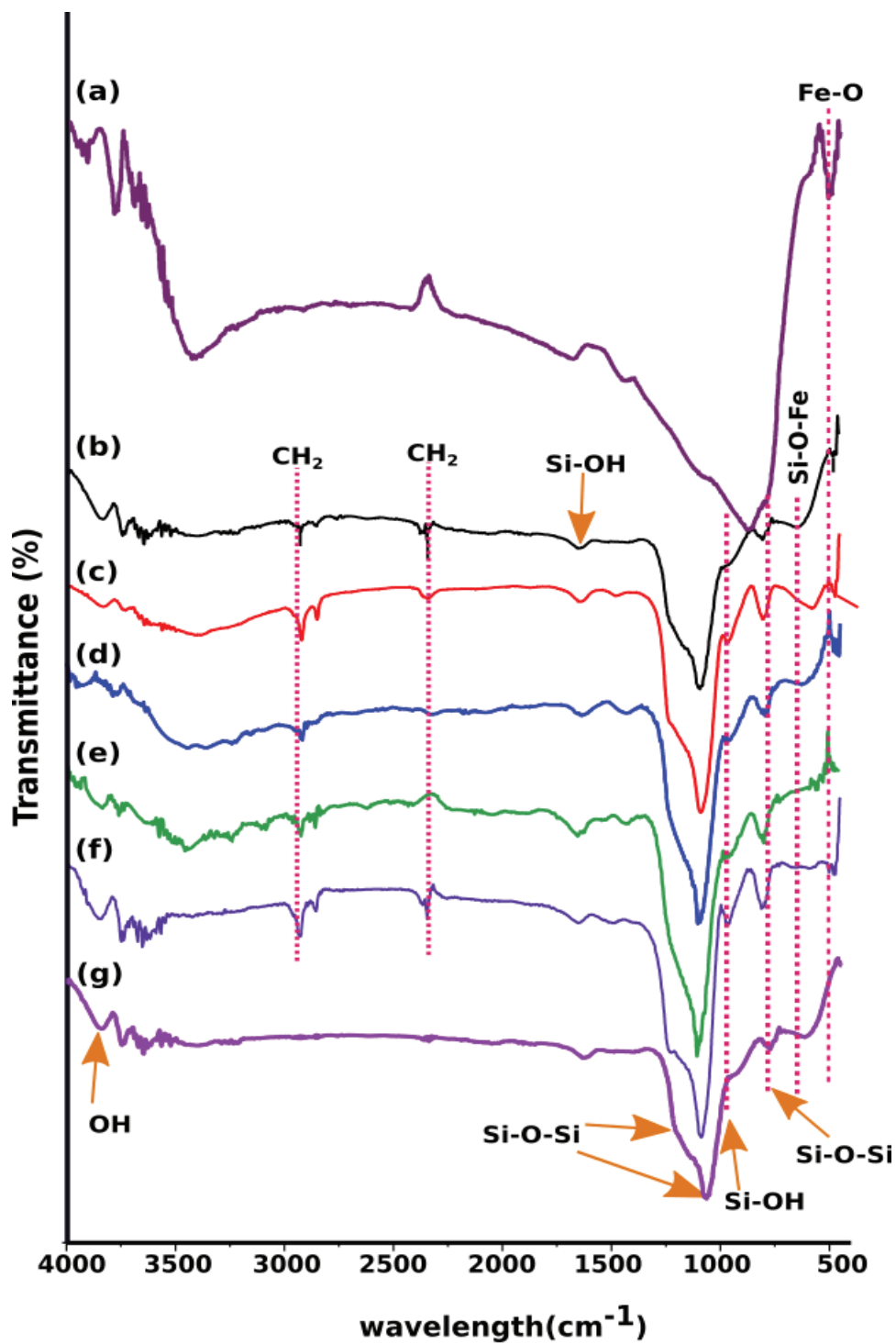


Figure 1: FTIR Spectra for (a) Fe₃O₄-NPs, Fe₃O₄@SiO₂ with Different Volumes of TEOS; (b) C1, (c) C3, (d) C5, (e) C7, (f) C9 and (g) Fe₃O₄@SiO₂ After CTAB Removal

Transmission Electron Microscopy (TEM)

Typical TEM images of $\text{Fe}_3\text{O}_4@\text{SiO}_2$ prepared using our simplified method are shown in Figure 2. The presence of the silica layer was confirmed with the morphology of $\text{Fe}_3\text{O}_4@\text{SiO}_2$ observed to be spherical. No defined morphology is observed in Figure 2(a). Samples C3, C5, C7 and C9 exhibited agglomerated spherical morphology.

We obtained the best results when 500 μL TEOS was used (sample C5), which produced nanoparticles with irregular magnetite core and spherical shaped silica shells. It shows the distribution of iron oxide nanoparticles (multiple darker spots) within the silica matrix (grey area).

Since the sample in Figure 2 (c) is mostly well encapsulated, it is easy to determine the average of silica thickness. The average silica thickness was measured to be around 70 nm with the Fe_3O_4 core measured to be 16 nm, which gave an average nanoparticle size of 86 nm.

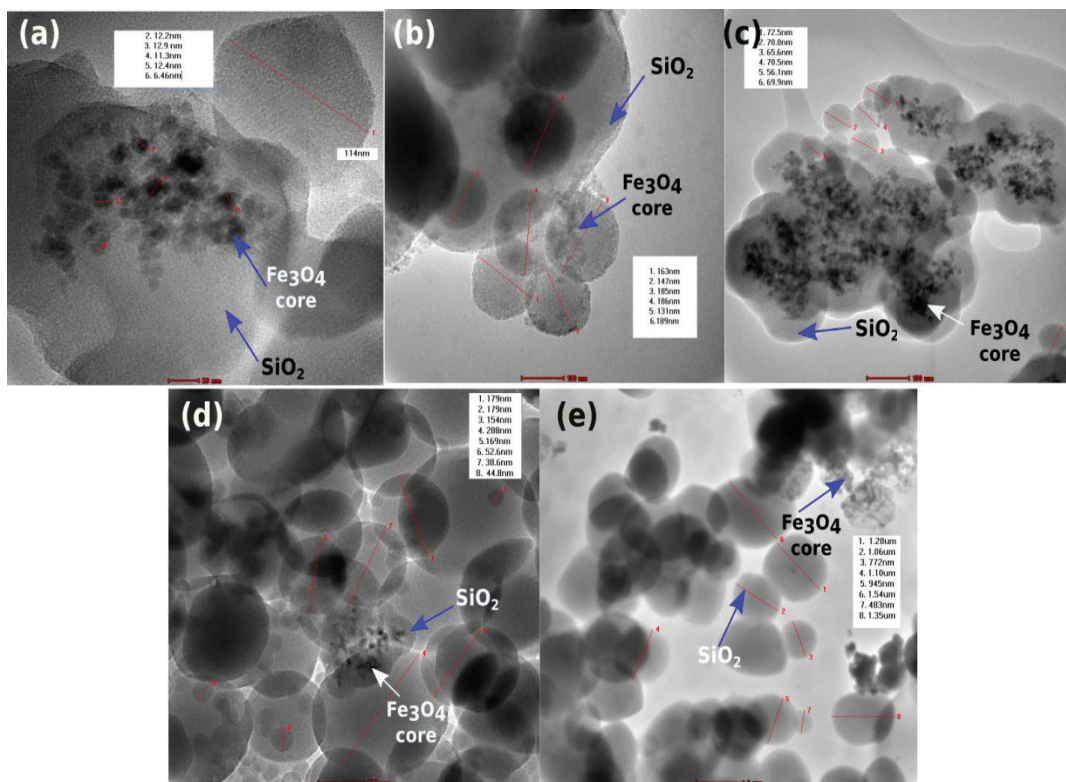


Figure 2: TEM Images of $\text{Fe}_3\text{O}_4@\text{SiO}_2$; (a) C1, (b) C3, (c) C5, (d) C7 and (e) C9. Scale bars: (a) 20 nm, (b) 100 nm, (c) 100 nm, (d) 100 nm and (e) 1 μLm

Field Emission Scanning Electron Microscopy (FESEM)

Figure 3 shows the smooth and spherical morphology of $\text{Fe}_3\text{O}_4@\text{SiO}_2$ nanoparticles produced. While agglomeration of particles a variety of size distributions of most grains are observed, the irregular arrangements led to a material whose size is still in the dimension of nanometers.

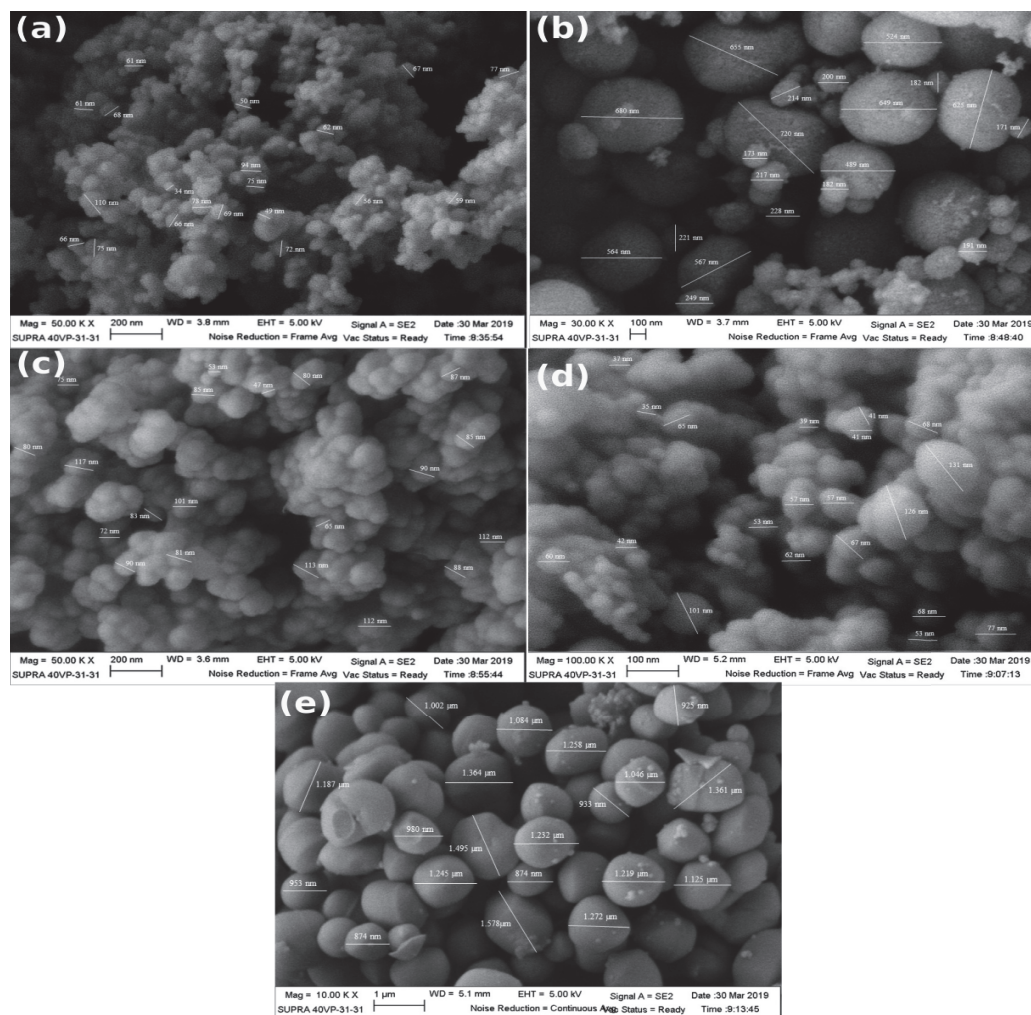


Figure 3: FESEM Micrograph of the $\text{Fe}_3\text{O}_4@\text{SiO}_2$ Prepared at Different Volume of TEOS; (a) C1, (b) C3, (c) C5, (d) C7 and (e) C9. Scale Bars: (a) 200 nm, (b) 100 nm, (c) 200 nm, (d) 100 nm and (e) $1\mu\text{Lm}$

The results confirmed the general inference that the size of the silica nanoparticles increases gradually with the volume of TEOS in the range $100\ \mu\text{L} - 900\ \mu\text{L}$ at $500\ \mu\text{L}$ of Fe_3O_4 NPs, $350\ \mu\text{L}$ of NaOH and $3\ \text{mL}$ of ethyl acetate (see Figure 3; Table 2).

It is also noticeable from Figure 3 (a) that monodisperse uniform-sized $\text{Fe}_3\text{O}_4@\text{SiO}_2$ nanoparticles of size 34-77 nm were obtained at low volume of TEOS (100 μL). Particles increased significantly to the range of 847-1578 nm when 900 μL of TEOS was used (Figure 3 (e)). It was observed that when 500 μL of TEOS were used, the iron oxide nanoparticles encapsulated within silica had a particle size ranging from 47 to 117 nm and were well monodispersed.

Table 2: Size of $\text{Fe}_3\text{O}_4@\text{SiO}_2$ Nanoparticles (Based on Micrographs)

Samples	Size of $\text{Fe}_3\text{O}_4@\text{SiO}_2$ nanoparticles
C1	34 – 78 nm
C3	171 – 720 nm
C5	47 -117 nm
C7	37 – 131 nm
C9	847 – 1578 nm

This is in good agreement with Bogush *et al.* [23], who reported larger particles produced with the increasing amount of TEOS. This result contradicts with van Helden *et al.* [24], who found that the particle size decreased as the volume of TEOS increases. However, according to Stober *et al.* [25], there was no effect of TEOS on final particle size.

This observation can be explained with the increasing volume of TEOS, the quantity of silica increases, it enhances the rate of both hydrolysis and condensation [26] and hence, bigger particles formed. The rate of formation of intermediate $[\text{Si}(\text{OC}_2\text{H}_5)_{4-x}(\text{OH})_x]$ will increase. Once it reaches the supersaturation region, the consumption rate of intermediate through condensation reaction is also relatively fast [27], which probably shortens the nucleation period. This will decrease the formation of nuclei and consequently the size of silica will become larger. Since the water and TEOS content required for hydrolysis is sufficiently high, the particle growth mechanism is more dominant, resulting in the increased particle size.

Energy Dispersive X-Rays Analysis (EDX)

EDX spectra showed the existence of elements Si (silicon), Fe (iron) and O (oxygen) and thus confirming the chemical composition of $\text{Fe}_3\text{O}_4@\text{SiO}_2$ (Figure 4). The presence of iron (Fe) was confirmed by the distinctive peak, approximately at 0.6 keV in all prepared $\text{Fe}_3\text{O}_4@\text{SiO}_2$ nanoparticles. Undoubtedly, the elements Si and O were due to the formation of siloxane bonds (Si-O-Si) and silanol group (Si-OH) indicate the effective coating of the magnetite nanoparticles with a silica layer. The low intensity of the Fe signal, which is attributed to the fact that most of the Fe_3O_4 -NPs are embedded within the silica and not on the surface.

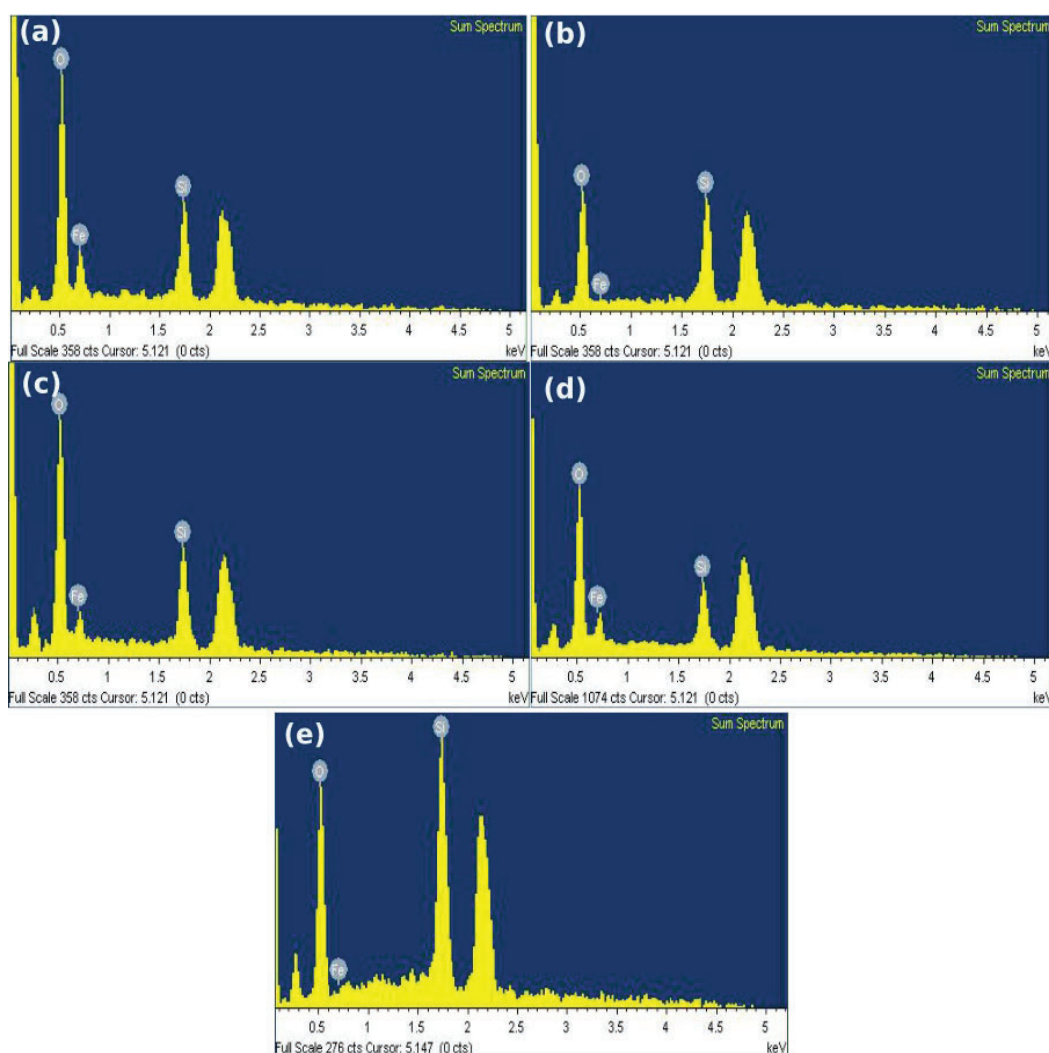


Figure 4: Energy Dispersive X-ray Spectroscopy (EDX) Analysis Spectra of the $\text{Fe}_3\text{O}_4@\text{SiO}_2$ Prepared at Different Volume of TEOS; (a) C1, (b) C3, (c) C5, (d) C7 and (e) C9

Magnetic Studies of Fe₃O₄@SiO₂ Nanoparticles

The magnetisation curves indicate that all the samples display a typical feature of superparamagnetism with approximately zero remanence and coercivity with no hysteresis being detected at room temperature (see Figure 5; Table 3).

It also can be found that the Fe₃O₄@SiO₂ prepared with different volume of TEOS of 100 μ L , 300 μ L , 500 μ L , 700 μ L and 900 μ L had saturation magnetisation (M_s) at 300K of about 22.0, 9.6, 43.3, 4.2 and 3.8 emu/g, respectively. The magnetisation value of the nanoparticles decreases dramatically upon the increasing volume of TEOS with the exception for sample C5, which had the highest magnetisation value.

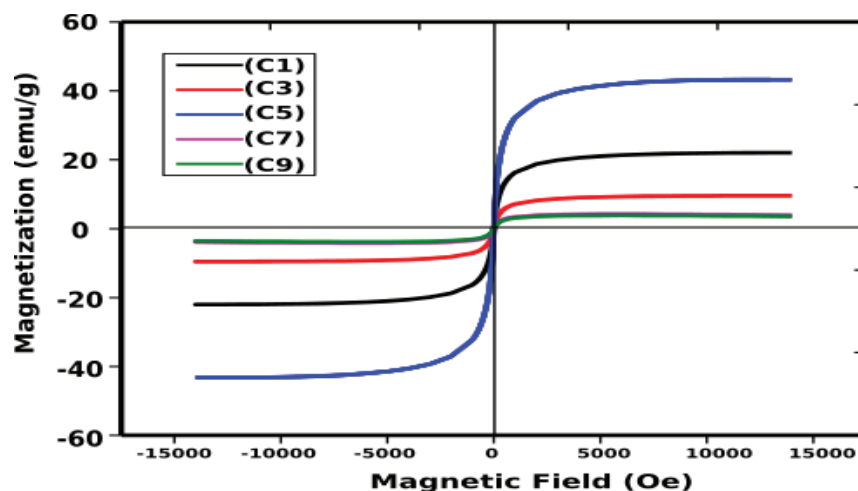


Figure 5: The Magnetisation Curves at Room Temperature for Fe₃O₄@SiO₂ with Different Volumes of TEOS; C1, C3, C5, C7 and C9

Table 3: Magnetic Values of the Fe₃O₄@SiO₂ Prepared at Different Volumes of TEOS

Samples	Saturation magnetisation (Ms) (emu/g)	Remnant magnetisation (Mr) (emu/g)	Coercivity (Hc)(Oe)	Squareness ratio (Mr/Ms)
C1	22.0	0.189	2.70	8.58×10^{-3}
C3	9.56	81.6×10^{-3}	2.74	8.53×10^{-3}
C5	43.3	0.419	2.94	9.67×10^{-3}
C7	4.20	41.4×10^{-3}	2.87	9.84×10^{-3}
C9	3.85	39.9×10^{-3}	3.14	1.04×10^{-2}

The presence of silica results in a lower saturation magnetisation (M_s) of the $\text{Fe}_3\text{O}_4@\text{SiO}_2$ than that of our synthesized Fe_3O_4 NPs [16]. This might be a result of the higher concentration of silica coating (nonmagnetic materials) on the surface of iron oxide nanoparticles, which might quench the magnetic moment [27]. This might be explained by the reduction of the energy associated with the particle–particle interaction and exchange coupling [28]. This behavior is expected once a nonmagnetic content such as SiO_2 was added to the system [29]. As the ratio of M_r to M_s is lower than 0.015, this result suggests that all the nanoparticles are superparamagnetic [30]. It is an important requirement for materials to have high saturation magnetisation and superparamagnetism for biomedical applications. Therefore, these $\text{Fe}_3\text{O}_4@\text{SiO}_2$ samples are having sufficient magnetisation that could be used for hyperthermia, magnetic resonance imaging (MRI) and magnetic drug targeting.

CONCLUSION

Silica-coated iron oxide nanoparticles ($\text{Fe}_3\text{O}_4@\text{SiO}_2$) were successfully synthesized using hydrolysis and condensation of tetraethyl orthosilicate (TEOS) under alkaline medium conditions at 80°C . The synthesized nanoparticles were characterised by using FTIR, TEM, FESEM-EDX and VSM. FESEM showed that the morphology of all samples has almost spherical structure of nanoparticles, whose particle size roughly increased with increasing volume of TEOS used in the synthesis. It was found that only $500\ \mu\text{L}$ of TEOS is required to obtain the best silica-coating on Fe_3O_4 core structures, confirmed by TEM and SEM analysis. TEM image revealed that some of Fe_3O_4 -NPs were encapsulated within the silica shell. EDX and FTIR analyses collectively suggest the existence of Si and Si-O confirming that the silica had been formed onto the surface of the iron oxide nanoparticles. All spherical silica nanoparticles were superparamagnetic at room temperature which suggests that the nanoparticles can be exploited for biomedical applications such as magnetic targeting drug delivery systems or magnetically-assisted applications.

ACKNOWLEDGEMENTS

Funding from Universiti Teknologi MARA (UiTM), Malaysia and Ministry of Higher Education (MOHE) (600-IRMI/FRGS 5/3 (046/2017)) are gratefully acknowledged. VSM was carried out using facilities at Universiti Kebangsaan Malaysia.

REFERENCES

- [1] M. Mahmoudi, S. Sant, B. Wang, S. Laurent, T. Sen, 2011. Superparamagnetic iron oxide nanoparticles (SPIONs): Development, surface modification and applications in chemotherapy. *Advanced Drug Delivery Reviews*, 63(1-2), 24-46. <https://doi.org/10.1016/j.addr.2010.05.006>
- [2] Q.A. Pankhurst, J. Connolly, S.K. Jones, J. Dobson, 2003. Applications of magnetic nanoparticles in biomedicine. *Journal of Physics D: Applied Physics*, 36(13), R167-R181. <https://doi.org/10.1088/0022-3727/36/13/201>
- [3] R. Qiao, C. Yang, M. Gao, 2009. Superparamagnetic iron oxide nanoparticles: from preparations to in vivo MRI applications. *Journal of Materials Chemistry*, 35(2009), 6274-6293. <https://doi.org/10.1039/B902394A>
- [4] S. Laurent, D. Forge, M. Port, A. Roch, C. Robic, L.V. Elst, R.N. Muller, 2008. Magnetic iron oxide nanoparticles: Synthesis, stabilisation, vectorization, physicochemical characterisations, and biological applications. *Chemical Reviews*, 108(6), 2064-2110. <https://doi.org/10.1021/cr068445e>
- [5] J. Dobson, 2006. Magnetic nanoparticles for drug delivery. *Drug Development Research*, 67(1), 55-60. <https://doi.org/10.1002/ddr.20067>
- [6] S.C. McBain, H.H. Yiu, J. Dobson, 2008. Magnetic nanoparticles for gene and drug delivery. *International Journal of Nanomedicine*, 3(2), 169-180. <https://doi.org/10.2147/ijn.s1608>

- [7] J.K. Oh, J.M. Park, 2011. Iron oxide-based superparamagnetic polymeric nanomaterials: Design, preparation, and biomedical application. *Progress in Polymer Science*, 36(1) 168-189. <https://doi.org/10.1016/j.progpolymsci.2010.08.005>
- [8] C. Vogt, M.S. Toprak, S. Laurent, J.-L. Bridot, R.N. Muller, M. Muhammed, High quality and tuneable silica shell-magnetic core nanoparticles. *Journal of Nanoparticle Research*, 12, 1137-1147. <https://doi.org/10.1007/s11051-009-9661-7>
- [9] Y. Piao, A. Burns, J. Kim, U. Wiesner, T. Hyeon, 2008. Designed fabrication of silica-based nanostructured particle systems for nanomedicine applications. *Advanced Functional Materials*, 18(23), 3745-3758. <https://doi.org/10.1002/adfm.200800731>
- [10] I.I. Slowing, J.L. Vivero-Escoto, C.-W. Wu, V.S.-Y. Lin, 2008. Mesoporous silica nanoparticles as controlled release drug delivery and gene transfection carriers. *Advanced Drug Delivery Reviews*, 60(11), 1278-1288. <https://doi.org/10.1016/j.addr.2008.03.012>
- [11] J.E. Lee, N. Lee, H. Kim, J. Kim, S.H. Choi, J.H. Kim, T. Kim, I.C. Song, S.P. Park, W.K. Moon, T. Hyeon, 2010. Uniform mesoporous dye-doped silica nanoparticles decorated with multiple magnetite nanocrystals for simultaneous enhanced magnetic resonance imaging, fluorescence imaging, and drug delivery. *J Am Chem Soc*, 132(2), 552-557. <https://doi.org/10.1021/ja905793q>
- [12] F. Ye, S. Laurent, A. Fornara, L. Astolfi, J. Qin, A. Roch, A. Martini, M.S. Topraka, R.N. Muller, M. Muhammed, 2012. Uniform mesoporous silica coated iron oxide nanoparticles as a highly efficient, nontoxic MRI T₂ contrast agent with tunable proton relaxivities. *Contrast Media & Molecular Imaging*, 7(5), 460-468. <https://doi.org/10.1002/cmml.1473>
- [13] C. Zhang, B. Wangler, B. Morgenstern, H. Zentgraf, M. Eisenhut, H. Untenecker, R. Kruger, R. Huss, O.C. Seliger, O.W. Semmler, F. Kiessling, 2007. Silica-and alkoxy silane-coated ultrasmall superparamagnetic iron oxide particles: A promising tool to label

- cells for magnetic resonance imaging. *Langmuir*, 23(3), 1427-1434. <https://doi.org/10.1021/la061879k>
- [14] M. Liong, J. Lu, M. Kovichich, T. Xia, S.G. Ruehm, A.E. Nel, F. Tamanoi, J.I. Zink, 2008. Multifunctional inorganic nanoparticles for imaging, targeting, and drug delivery. *ACS Nano*, 2(5), 889-896. <https://doi.org/10.1021/nn800072t>
- [15] S. Laurent, S. Dutz, U.O. Häfeli, M. Mahmoudi, 2011. Magnetic fluid hyperthermia: Focus on superparamagnetic iron oxide nanoparticles. *Advances in Colloid and Interface Science*, 166(1-2), 8-23. <https://doi.org/10.1016/j.cis.2011.04.003>
- [16] N.I. Taib, F.A. Latif, Z. Mohamed, N.D.S. Zambri, 2018. Green synthesis of iron oxide nanoparticles (Fe₃O₄-NPs) using azadirachta indica aqueous leaf extract. *International Journal of Engineering & Technology*, 7(4.18), 9-13.
- [17] N.D.S. Zambri, N.I. Taib, F.A. Latif, Z. Mohamed, 2019. Utilization of neem leaf extract on biosynthesis of iron oxide nanoparticles. *Molecules*, 24(20), 3803. <https://doi.org/10.3390/molecules24203803>
- [18] Y.H. Lien, T.-M. Wu, 2008. Preparation and Characterisation of thermosensitive polymer grafted onto silica-coated iron oxide nanoparticles. *Journal of Colloid and Interface Science*, 326(2), 517-512. <https://doi.org/10.1016/j.jcis.2008.06.020>
- [19] N.I. Taib, S. Endud, M.N. Katun, 2012. XRD, FTIR and ¹³C CP/MAS NMR Studies of Composite comprising Poly(vinyl acetate)-silylated Si-MCM-41. *Advanced Materials Research*, 364, 159-163. <https://doi.org/10.4028/www.scientific.net/AMR.364.159>
- [20] F.E. Sangok, S.M. Yahaya, N.I. Taib, S.Z. Sa'ad, N.F. Rasarudin, 2012. Comparison study of amino-functionalized and mercaptopropyl-functionalized mesoporous silica MCM-41. *Advances in Chemical Engineering*, 550-553(July), 1603-1606. <https://doi.org/10.4028/www.scientific.net/AMR.550-553.1603>

- [21] N.I. Taib, S. Endud, M.N. Katun, 2011. Functionalisation of mesoporous Si-MCM-41 by grafting with trimethylchlorosilane. *International Journal of Chemistry*, 3(3), 2.
- [22] X.L. Liang, N. Bao, X. Luo, S.N. Ding, 2018. CdZnTeS quantum dots based electrochemiluminescent image immunoanalysis. *Biosens Bioelectron*, 117, 145-152. <https://doi.org/10.1016/j.bios.2018.06.006>
- [23] G.H. Bogush, M.A. Tracy, C.F.Z. Iv, 1988. Preparation of monodisperse silica particles: control of size and mass fraction. *Journal of Non-Crystalline Solids*, 104(1), 95-106. [https://doi.org/10.1016/0022-3093\(88\)90187-1](https://doi.org/10.1016/0022-3093(88)90187-1)
- [24] V. Helden, J.W.J. A. K., A. Vrij, 1981. Preparation and Characterisation of spherical monodisperse silica dispersions in nonaqueous solvents. *Journal of Colloid and Interface Science*, 81(2), 354-368. [https://doi.org/10.1016/0021-9797\(81\)90417-3](https://doi.org/10.1016/0021-9797(81)90417-3)
- [25] W. Stöber, A. Fink, E. Bohn, 1968. Controlled growth of monodisperse silica spheres in the micron size range. *Journal of Colloid and Interface Science*, 26(1), 62-69. [https://doi.org/10.1016/0021-9797\(68\)90272-5](https://doi.org/10.1016/0021-9797(68)90272-5)
- [26] G.H. Bogush, C.F.Z. Iv, 1991. Studies of the kinetics of the precipitation of uniform silica particles through the hydrolysis and condensation of silicon alkoxides. *Journal of Colloid and Interface Science*, 142(1), 1-18. [https://doi.org/10.1016/0021-9797\(91\)90029-8](https://doi.org/10.1016/0021-9797(91)90029-8)
- [27] S.-L. Chen, P. Dong, G.-H. Yang, J.-J. Yang, 1996. Kinetics of formation of monodisperse colloidal silica particles through the hydrolysis and condensation of tetraethylorthosilicate. *Industrial & Engineering Chemistry Research*, 35(12), 4487-4493. <https://doi.org/10.1021/ie9602217>
- [28] A.B. Salunkhe, V.M. Khot, N.D. Thorat, M.R. Phadatare, C.I. Sathish, D.S. Dhawale, S.H. Pawar, 2013. Polyvinyl alcohol functionalized cobalt ferrite nanoparticles for biomedical applications. *Applied Surface Science*, 264, 598-604. <https://doi.org/10.1016/j.apsusc.2012.10.073>

- [29] F.d. Monte, M.P. Morales, D. Levy, A. Fernandez, M. Ocaña, A. Roig, E. Molins, K. O'Grady, C.J. Serna, 1997. Formation of γ -Fe₂O₃ isolated nanoparticles in a silica matrix. *Langmuir*, 13(14), 3267-3634. <https://doi.org/10.1021/la9700228>
- [30] K. Tadyszak, A. Kertmen, E. Coy, R. Andruszkiewicz, S. Milewski, I. Kardava, B. Scheibee, S. Jurga, K. Chybczynska, 2017. Spectroscopic and magnetic studies of highly dispersible superparamagnetic silica coated magnetite nanoparticles. *Journal of Magnetism and Magnetic Materials*, 433, 254-261. <https://doi.org/10.1016/j.jmmm.2017.03.025>